RSC Advances

PAPER

View Article Online
View Journal | View Issue

Cite this: *RSC Adv.*, 2014, **4**, 64476

Identification of chemicals resulted in selective glycerol conversion as sustainable fuel on Pd-based anode nanocatalysts

L. M. Palma,[a] T. S. Almeida,[a] V. L. Oliveira,[b] G. Tremiliosi-Filho,[b] E. R. Gonzalez,[b] A. R. de Andrade,[a] K. Servat,[c] C. Morais,[c] T. W. Napporn[c] and K. B. Kokoh*[c]

Received 4th September 2014
Accepted 10th November 2014

DOI: 10.1039/c4ra09822f

www.rsc.org/advances

Palladium-based nanoparticles were prepared using mild microwave-assisted heating. The activity of carbon supported PdM (M = Mn and Fe) toward glycerol oxidation in alkaline medium was studied by coupling electrochemical, analytical and *in situ* spectroscopic techniques. The complementary findings showed that glycerol was converted into oxalate, tartronate, glycerate, glycolate and formate. The *ex situ* analytical methods (liquid chromatography and mass spectrometry) were helpful to reveal glycerate as the major reaction product on PdM/C anodes, while from *in situ* infrared spectroscopy measurements no irreversible adsorbed poisoning species was detected in glycerol or intermediate oxidation to carbonate at the prepared electrodes. The correlation of the analytical and physicochemical (XRD, EDX and TEM) results concerned the shift of the onset potential toward lower values and the high Faradaic currents due to electronic structures provided by the Mn and Fe contents to the Pd based materials. Accordingly, glycerol is a sustainable raw material, which can be used in cogeneration processes for renewable energy sources and selective production of added-value molecules.

1. Introduction

Glycerol is expected to play an important role in a CO_2-decoupled scenario, as it is recognized to be one of the promising sustainable organic compounds capable of supplying fuel direct alcohol fuel cell (DAFC) devices.[1–3] Indeed, to face the scarcity of fossil energy sources, the use of alternative fuels from renewable sources should be envisaged as an environmentally friendly approach. Glycerol is already used as raw material in various industrial applications.[4,5] But, as it represents 10% of the amount of the biodiesel production that is increasing because of the growing global energy demand,[6] the surplus glycerol can be used as fuel in solid polymer electrolyte fuel cell applications to make the increase economically viable.[7] Beyond the fact that it is a non-toxic liquid and easy to transport and handle, glycerol has a theoretical energy density (6.4 kWh L^{-1}).[3,8] In comparison with other fuels such as methanol and ethanol, glycerol has two major strengths: a high theoretical number of exchanged electrons (14 electrons per glycerol molecule) when converted thoroughly into CO_2, and an excellent source of production of added-value molecules in a selective oxidative conversion.[7] It was reported that glycerol oxidation led to dihydroxyacetone,[9–13] lactic,[14] mesoxalic,[15] glyceric,[16,17] glycolic,[18,19] tartronic[9] acids. From these previous reports, the distribution of the glycerol reaction products strongly depends on the material surface and can be associated with a cogenerating approach, which consists in both converting directly chemical energy to electrical energy, and recovering added-value chemicals from glycerol selective electrooxidation. Various materials based on platinum and gold[20–24] have been used as electrocatalysts in the glycerol oxidation in alkaline medium where many organics are very electroreactive because of the active metal hydroxide or oxide sites at the electrode surface. To some extent, bimetallic materials have the potential to enhance reaction rate, alter product selectivity, and/or help or prevent catalyst deactivation. The remarkable activity of palladium, which is close to that of platinum, makes it a promising material in catalysis and particularly in electrocatalysis[7,15,25–28] because it is 200 times more abundant on earth than platinum.[8,29,30] It was reported that the high activity and stability of palladium were due to its good poisoning resistance.[31] Platinum group metals (PGM) based multimetallic nanostructures with well-controlled size, shape, structure chemical composition and morphology can effectively enhance the catalytic reaction kinetics through modifying surface compositions, optimizing highly active crystalline facets, and tuning electronic structures.[30,32–34] Indeed, the addition of a co-catalyst such as nickel,

[a]*Departamento de Química da Faculdade de Filosofia Ciências e Letras de Ribeirão Preto, Universidade de São Paulo, Av. Bandeirantes, 3900, 14040-901, Ribeirão Preto, SP, Brazil*

[b]*Instituto de Química de São Carlos, Universidade de São Paulo, C.P. 780, 13560-970 São Carlos, SP, Brazil*

[c]*Université de Poitiers, UMR CNRS 7285, « Equipe SAMCat », 4, rue Michel Brunet, B27, TSA 51106, 86073 Poitiers Cedex 09, France. E-mail: boniface.kokoh@univ-poitiers.fr*

silver, *etc.*, to Pd-based anodes results in a beneficial electronic effect evidenced by an onset potential shifted toward lower values, high current densities, and CO removal from the electrode surface at lower potentials.[35–42] In this work we show an oxidative transformation of glycerol when the Pd electrode surface is modified by Mn and Fe elements. Investigations were focused on the identification of the main reaction products with an analytical setup composed of *in situ* infrared reflectance spectroscopy, liquid chromatography (LC) and LC-Mass Spectrometry.

2. Results and discussion

2.1 Physicochemical characterization of the nanomaterials

The carbon supported Pd-based nanomaterials obtained through microwave-assisted heating (MW) were first characterized physicochemically by XRD and TEM techniques.

The XRD patterns of PdM/C (M = Fe, Mn) are displayed in Fig. 1. As can be seen, all the XRD patterns have similar characteristic peak positions attributed to a face-centred-cubic (fcc/$Fm\bar{3}m$) palladium structure. Indeed, the peaks at 40.25, 46.5 and 68.08 and 83.02° represent respectively the (111), (200), (220) and (311) reflection planes of a Pd crystallite.

All the samples also show a broad peak at 25.1°, which is assigned to the (002) plane of carbon graphite issued from the support used to disperse the metal loading. The diffractogram of Pd containing the iron element displays other peaks at 35, 57 and 63° which can be attributed to the Fe_2O_3 phases. Although the diffractogram of the PdMn/C material does not exhibit any peak related to the Mn element, as already described in the literature,[19,43,44] TEM and EDX analyses provided evidences of the presence of Mn oxides. They are probably not well crystallized, but under amorphous form, because of the microwave-assisted approach undertaken without ultimate heat-treatment stage.

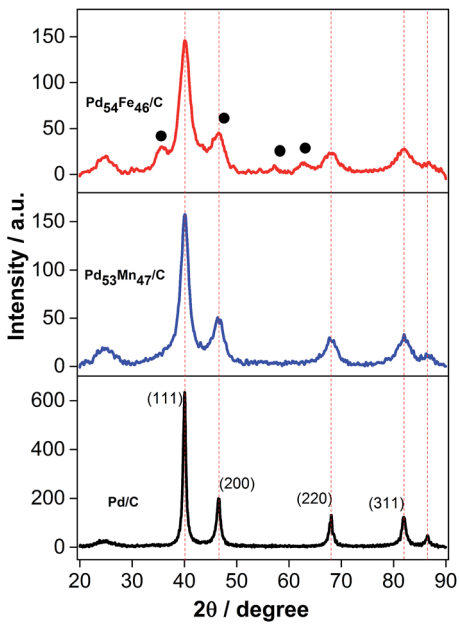

Fig. 1 XRD patterns of the PdM (M = Mn and Fe) nanomaterials prepared by MW process and dispersed on Vulcan XC-72 carbon; (●) Fe_2O_3 phase.

Crystallite sizes estimated by the Scherrer equation on the well-defined (200) peak are lying between 3 and 7 nm. These size values are similar to those of other catalysts prepared by microwave-assisted heating.[45,46] EDX analysis confirmed the presence of bimetallic catalysts in each sample and Table 1 shows that the average atomic compositions of the different materials are close to the nominal ones. Their lattice parameters are also close to that of the Pd crystallite (a_{Pd} = 3.89 Å), indicating *a priori* no substantial deformation of the initial structure, with the insertion of another metal in the Pd crystalline structure.

Fig. 2 shows representative TEM images and histograms obtained for the PdM/C materials. The Pd/C material present clusters of particles from 10 to several hundred nanometers in diameter (D_{TEM}), and small particles ranging from 3–40 nm in diameter. The distribution of the metallic phase and particle size is heterogeneous on the carbon support, and the average particle size is 4.2 nm. $Pd_{53}Mn_{47}$/C catalysts are distributed in two forms: particles of pure Pd with diameter between 2 to 4 nm, and rods of Mn_xO_y. Pd particles appear either onto the carbon or Mn_xO_y, and the average particle size is 3.8 nm. $Pd_{54}Fe_{46}$/C catalysts also show two different distinct structures on TEM images: spheres of Pd with diameter between 2 to 4 nm, and clusters constituted mainly of Fe_2O_3 with 4 to 10 nm of diameter. Both metals can also be found in the same cluster, and the metallic phase is well distributed on the carbon support; the average particle size is 4.8 nm (Table 1), indicating a fair line with the crystallite sizes obtained from XRD analysis.

2.2 Electrochemical and analytical measurements

Glycerol oxidation was conducted in a two-compartment cell separated with a Fumatech anion exchange membrane. Prior to long-term chronoamperometric tests, a cyclic voltammogram of each anode catalyst was recorded for evaluating the electrochemical behaviour of the molecule at the material surface. As shown in Fig. 3, one intense oxidation peak is observed during the forward potential scan. This peak takes place at *ca.* 0.9 V *vs.* RHE on the Pd/C electrode. When the latter material is modified by either Mn or Fe elements the onset potential shifts towards lower values, indicating its beneficial effect on Pd towards glycerol electrooxidation. The presence of the Mn element in the catalyst composition increases the current densities and leads to a larger potential domain of the glycerol oxidation. Although the increase in the current density is lower for the

Table 1 XRD and EDX results for the prepared nanomaterials

Material					
Nominal	Experimental	Phase	a/Å	D_{DRX} (200)/nm	D_{TEM}/nm
Pd/C	Pd/C	Pd	3.89	6.87	6.16
$Pd_{50}Fe_{50}$/C	$Pd_{54}Fe_{46}$/C	Pd	3.89	3.12	4.82
$Pd_{50}Mn_{50}$/C	$Pd_{53}Mn_{47}$/C	Pd	3.89	4.90	3.81

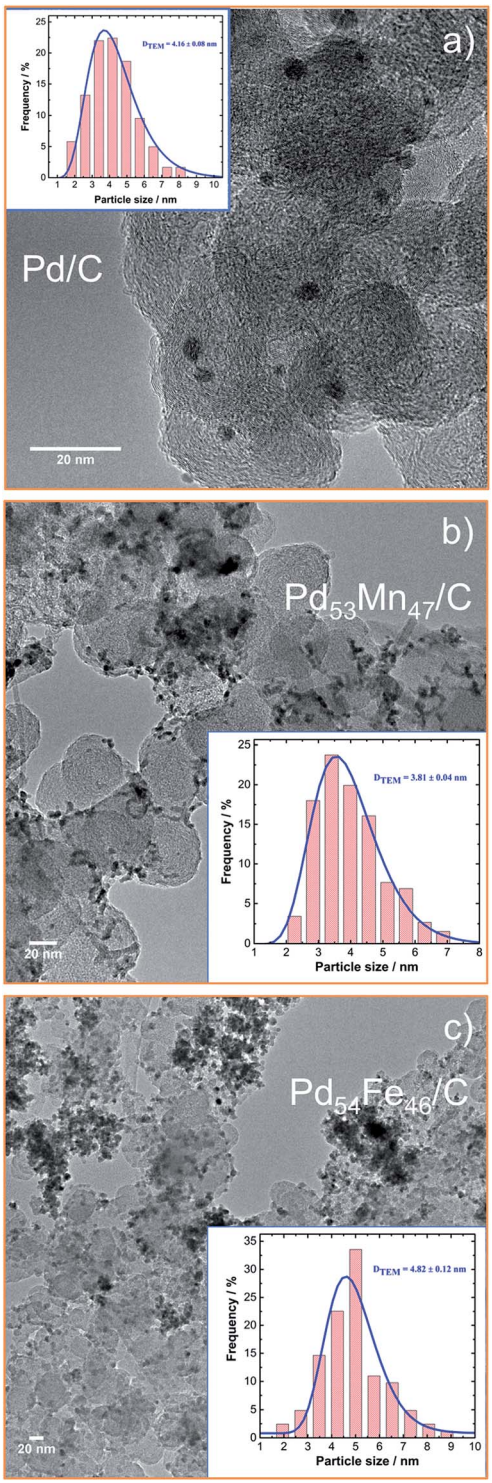

Fig. 2 TEM images of the PdM/C (M = Mn and Fe) nanomaterials prepared by the MW method. The insets represent the histograms of the particle size distribution.

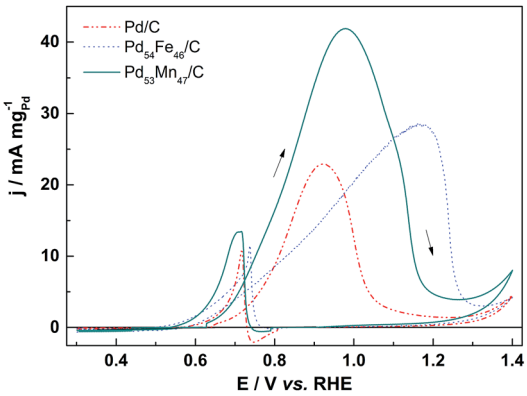

Fig. 3 Cyclic voltammograms of the PdM/C (M = Mn and Fe) electrocatalysts in 0.1 M NaOH containing 0.1 M glycerol, recorded at 5 mV s^{-1}.

Fe-containing material the glycerol oxidation domain remains still larger, ranging from 0.6 to *ca.* 1.3 V *vs.* RHE. Addition of the oxophilic metal to a catalyst composition is of great interest not only to decrease the noble metal content, but also to nucleate adsorbed hydroxides at potentials less positive than those on bare Pd; hence this facilitates the initial molecule and intermediates oxidative removal from the electrode surface.[30,47] During the negative going-scan the second glycerol oxidation peak takes place earlier and/or has higher current densities on PdM/C than on Pd/C. This is probably due to the presence of active Mn and Fe oxide/hydroxide species at the Pd-based electrode surface in this potential domain. Song *et al.*[48] have shown that PdFe/C catalysts were not active to the oxidation of alcohols such as methanol and ethanol in acidic medium. Taking into account that glycerol contains similar primary alcohol groups and the current densities obtained herein, it can be concluded that the alkaline electrolyte does have a contribution in the activation of the molecule in the presence of oxygenated species at the PdM (M = Mn and Fe) electrode surface.

Regarding these different electroreactivities of glycerol at the Pd-based anodes, chronoamperometry experiments were performed at 0.8 V *vs.* RHE during 4 h. These long-term electrolyses provide helpful information on the durability of the catalyst in direct glycerol fuel cell, and also permit to determine the main resulted reaction products in a cogeneration glycerol process on such PdM/C anode catalysts. Accordingly, at the end of each electrolysis the bulk solution of the anodic compartment was recovered and divided in two parts.

The first volume was sampled in liquid chromatography to determine the amounts of the reaction products by comparison with commercial standards. Fig. 4 shows the results of the chromatograms in terms of the products obtained in the glycerol oxidation on the different Pd-based electrode materials. Oxalate, tartronate, glycerate, glycolate and formate are detected in the bulk solution after 4 h glycerol oxidation. Although the same products are formed on Pd-based catalysts, glycerate remains, whatever the electrode, the main organic compound. It is worthy of note that the chromatographic peak of oxalate overlaps partially the injection peak, preventing under these analytical conditions the accurate quantification of its amount.

Under similar mild conditions, these reaction products were also found on Au/C catalysts, except for the presence in small

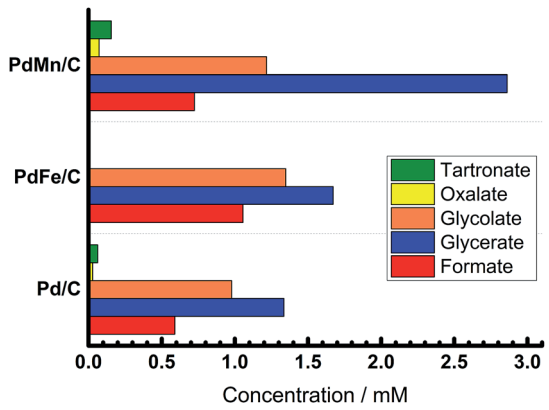

Fig. 4 Distribution of the glycerol oxidation products after 4 h electrolysis performed at 0.8 V *vs.* RHE on PdM/C (M = Mn and Fe) electrocatalysts in 0.1 M NaOH.

amounts of mesoxalate and lactate reported on Au/C materials.[22,49]

The second volume of electrolytic solution was first neutralized on an ion exchange resin (Dowex). It consists briefly in regenerating the as-received resin with 0.5 M H_2SO_4 and then washing it until obtaining a neutral pH. Afterwards the electrolytic solution was passed through the resin to neutralize the supporting electrolyte (NaOH) and thereby the carboxylate ions become carboxylic acids. To be sure to recover all the compounds an equivalent volume of water was added on the resin. The pretreated solution was injected on an Aminex column (HPX-87H) connected to the mass spectrometer as detector. The samples obtained from glycerol electrooxidation on Pd/C, PdMn/C and PdFe/C gave qualitatively the same spectrograms; the representative one PdMn/C is shown in Fig. 5.

Glyceric acid is the main reaction product well identified with $m/z = 105$, which corresponds to the molecular weight without a proton. Oxalic acid is also determined by its mass spectrum ($m/z = 89$), as depicted in Fig. 5. The same molecules were found on spectrograms recorded with the electrolytic solution issued from the glycerol oxidation on Pd/C and PdFe/C.

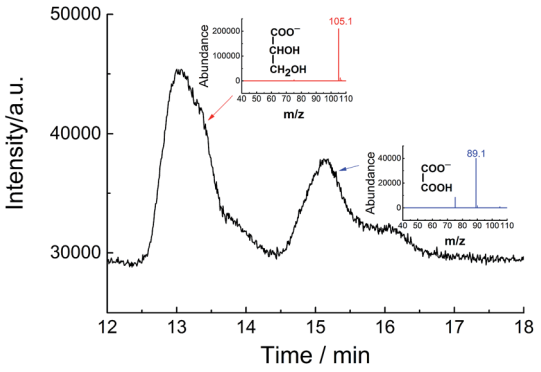

Fig. 5 Representative mass spectra of the main molecules resulting from the glycerol oxidation performed at 0.8 V *vs.* RHE on PdMn/C electrocatalyst.

2.3 Spectroelectrochemical identification of the products

To get further insights on how glycerol is electrooxidized in alkaline medium on these nanoscale PdM/C materials, *in situ* Fourier Transform Infrared Spectroscopy (FTIRS) experiments were undertaken. These *in situ* spectroelectrochemical measurements allow detection of intermediates and reaction products in very small amounts and will hopefully provide supplementary insights to LC-MS findings on the glycerol oxidation. In Fig. 6 are depicted the single potential alteration infrared (SPAIR) spectra obtained for the different Pd-based/C catalysts. Reflectivities were recorded at 50 second intervals during the glycerol electrooxidation in alkaline medium (0.1 M NaOH) at a sweep rate of 1 mV s^{-1}. These spectra will allow correlating the appearance and/or disappearance of certain characteristic vibration bands to the potential applied to the working electrode.

The first important outcome is the evidence of CO_2 (asymmetric stretching band at 2343 cm^{-1}) production on the Pd/C and PdFe/C nanocatalysts at about 1.0 V *vs.* RHE. Indeed, CO_2 appears as soon as carbonate (1390–1420 cm^{-1}) could not be further formed due to the lack of OH^- indicating therefore an acidification of the medium. It has been shown by simple calculation that the depletion of OH^- in the thin layer (window-electrode interface) is enough to justify a pH change during glycerol electrooxidation in alkaline medium.[50] The acidification of the thin layer between the working electrode and the CaF_2 window is therefore clearly shown. Another point is that no vibration band indicating the presence of corresponding linear or bridged CO was observed.

Based on the obtained spectra an attempt to identify the reaction intermediates will be now undertaken. The positive bands at 1050, 1900 and 2700 cm^{-1} observed in the different FTIR spectra are attributed to glycerol and OH^- consumption, whereas the positive band appearing at *ca.* 1640 cm^{-1} corresponds to water bending vibration. The characteristic FTIR spectra of the different possible products or intermediates recorded in alkaline medium have been published elsewhere[51] and will be used herein to conclude on their presence in the electrolytic solution. So, for the Pd/C catalyst several

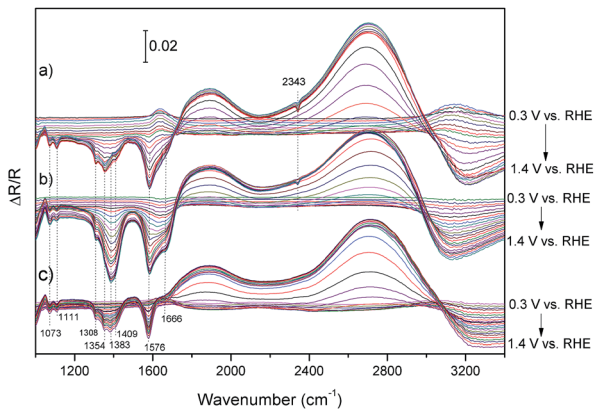

Fig. 6 SPAIR spectra recorded during glycerol (0.1 M) oxidation on Pd/C (a), PdFe/C (b) and PdMn/C (c) electrocatalysts in 0.1 M NaOH.

compounds could be evidenced at potential values above 0.8 V *vs.* RHE, namely glycerate (characteristic bands at 1111 and 1409 cm^{-1}), glycolate (characteristic bands at 1073, 1324 and 1409 cm^{-1}) oxalate (sharp band at 1308 cm^{-1}) and formate (1354, 1383 cm^{-1}). No band characteristic of tartronate and/or mesoxalate ions (characteristic IR bands at 1100, 1338 and 1438 cm^{-1}) was observed but their presence in very little amounts in the thin layer electrolyte solution cannot be excluded. It should be stated that the intense band at 1576 cm^{-1} is characteristic of different carboxylate ions and there also might be a contribution of the water bending vibration to this band. For potential values higher than 1.0 V *vs.* RHE CO_2 formation takes place while the amounts of formate, glycolate and oxalate (region from 1308 to 1410 cm^{-1}) increase. This indicates therefore the transformation at high potential values of glycerate into glycolate and/or formate with the formation of adsorbed CO that is immediately oxidized to carbonate or CO_2, depending on the pH, according to the mechanism proposed in ref. 51. Finally, a broad vibration band is also clearly visible at *ca.* 1666 cm^{-1} that might be attributed to adsorbed glyceraldehyde or carbonyl species. The same reaction intermediates were identified when using bimetallic materials as electrocatalysts. The major differences occur at high potential values. Indeed, the spectra obtained at high potential values for the PdFe/C material indicate that the oxidation of glycerate occurs preferentially following the glycolate pathway with the formation of large amounts of carbonyl species (1666 cm^{-1}) and subsequently high amounts of carbonate (1390–1420 cm^{-1}) and/or CO_2 (2343 cm^{-1}). For the PdMn/C material the oxidation into formate (1354 and 1383 cm^{-1}) is predominant. Based on these results we can therefore state that the pathway for the electrooxidation of glycerol on PdM/C materials in alkaline medium is the glyceraldehyde one and the major reaction products are glycerate, glycolate and formate.

An *in situ* IR study coupled with chronoamperometry experiments has also been performed. Chronoamperometry was carried out during one hour at 0.8 V *vs.* RHE in the presence of 0.1 mol L^{-1} glycerol in alkaline medium. The spectra obtained after 30 minutes are plotted in Fig. 7 for the three studied catalysts. The absence of the band at 2343 cm^{-1} confirms the hypothesis that carbon dioxide is produced from the oxidation of adsorbed species at high potential values. Another point is the enhancement of some vibration bands that might be assigned to adsorbed species, confirming therefore the progressive poisoning of the catalysts. Indeed, the band at 1680 cm^{-1} has been assigned to adsorbed glyceraldehyde and carbonyl species whereas the band at *ca.* 1380 cm^{-1} has been shown to be characteristic of adsorbed glycerate.

Chronoamperometry experiments coupled with *in situ* FTIR measurements confirm therefore the glyceraldehyde pathway for the glycerol electrooxidation in alkaline medium on Pd-based materials bringing to light adsorbed glyceraldehyde and glycerate as main intermediates.

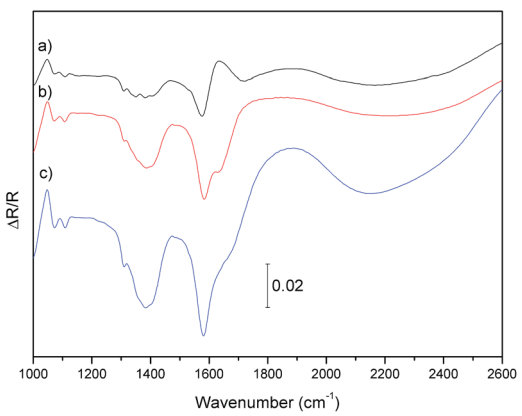

Fig. 7 FTIR spectra of the species recorded after 30 minutes of chronoamperometry measurements performed at 0.8 V *vs.* RHE on Pd/C (a), PdFe (b) and PdMn (c) electrocatalysts in 0.1 M NaOH containing 0.1 M glycerol.

3. Experimental

Electrocatalysts with nominal composition PdM/C (50 : 50), M = Fe, and Mn, were prepared by microwave-assisted heating (MW).[52] The nanocatalysts were obtained by mixing $PdCl_2$ (Aldrich) aqueous solution with the appropriate amount of $FeCl_3 \cdot 6H_2O$ (Sigma Aldrich) or $MnCl_2 \cdot 4H_2O$ (Sigma Aldrich) alcoholic solution in 30 mL of propylene glycol. Sodium hydroxide was added to the mixture, to increase the pH approximately to 10; it also acts as stabilizing agent. The mixture was stirred for 10 min in an ultrasonic bath. Next, enough pre-treated Vulcan XC-72 carbon powder was added, to obtain electrocatalysts with 40 wt% metal loading. Ultrasound irradiation for 50 min provided a homogeneous suspension, which was placed in a common commercial microwave oven (Panasonic NN-ST568WRU, 2450 Hz, 800 W) for 1 min on, 10 s off, 1 min on. Finally, the suspension was filtered and washed with acetone (Merck), and the solid product was dried in an oven at 120 °C for 2 h, under N_2 atmosphere.

3.1 Physical characterization

The diffraction patterns of the electrocatalysts were obtained on an X-ray diffractometer (D5005 Siemens) operating with Cu Kα radiation (λ = 1.5406 Å) generated at 40 kV and 40 mA. The following parameters were kept constant during the analysis: 2θ range = 20–90°, step = 0.03°, and total analysis time = 1.97 h. Catalyst phase composition and analysis of the position relative to the Kα1 monochromatic radiation were achieved by fitting the experimental angular range of interest to the pseudo-Voigt function per crystalline peak with the aid of the Profile Plus program (Siemens AG). The crystallite size values were obtained using the Debye–Scherrer equation.[53] Details of the procedure have been described previously.[54] The unit cell parameters were determined by a computer program (U-Fit.exe v1.3-1992) using the least-squares method. The 2θ experimental values and the reflection planes ($h\,k\,l$) were employed, to calculate the unit cell.

Energy dispersive X-ray (EDX) analysis using a Leica microscope Zeiss LEO 440 model TEM coupled to an Oxford 7060

model analyzer was used to determine the chemical composition and homogeneity of the nanomaterials.

The morphology of the electrocatalysts was also investigated by Transmission Electron Microscopy (TEM) using a TEM/STEM JEOL 2100 UHR microscope (200 kV) equipped with a LaB_6 filament. The mean particle size and size distribution were determined by measuring the diameter of an average of 200 isolated particles using ImageJ software.

3.2 Electrochemical measurements

Chronoamperometry measurements were carried out in a Pyrex two-compartment cell. The compartments were separated with an anion-exchange membrane (35 μm thickness, from Fumatech) and were deaerated by ultrapure N_2 (U Quality, from l'Air Liquide). A Reversible Hydrogen Electrode (RHE) and slab of vitreous carbon were used as reference and counter electrode, respectively. The reference electrode was separated from the solution by a Luggin–Haber capillary tip.

The working electrode consisted of catalytic powders deposited on a Carbon Toray used as conductive carrier with a geometric surface area of 3 cm^2. The electrical connection of the carbon Toray substrate was established with a gold wire using a carbon paste. A catalytic ink was prepared from the metal/C powder (2 mg) added in a mixture of 425 μL of Nafion® suspension (Aldrich) and 75 μL of water. 50 μL of the catalytic ink was finally deposited onto each face of the carbon Toray sheet and the solvent was evaporated at room temperature; this amount represents 133 μg cm^{-2} of metal loading.

A conventional three-electrode electrochemical cell (50 mL) was used for the CV electrochemical measurements conducted on an Autolab (PGSTAT-30) Potentiostat. The ink consisting of an appropriate amount of the electrocatalyst powder, isopropyl alcohol (99 μL), and Nafion® (1 μL) (5 wt% in aliphatic alcohols, Aldrich) was homogenized in ultrasonic bath for 60 min. A mass density of 0.32 mg_{Pd} cm^{-2} was deposited onto a previously polished glassy carbon electrode (area = 0.07 cm^2).

All the catalysts were characterized in alkaline medium (0.1 mol L^{-1} NaOH – Merck), and in the presence of glycerol (0.1 mol L^{-1} – Sigma-Aldrich). Cyclic voltammetry in the potential range 0.1 to 1.40 V *vs.* RHE and chronoamperometry at 0.8 V *vs.* RHE for four hours, was performed in order to determine the products formed.

3.3 Fourier transform infrared spectroscopy measurements

In situ FTIR experiments were carried out under external reflection conditions in a Bruker IFS 66v spectrometer which was modified for beam reflection on the electrode surface at a 65° incidence angle. The detector was a MCT (HgCdTe), beforehand cooled by liquid nitrogen. To avoid the presence of IR bands due to atmospheric CO_2 and H_2O, the system was maintained under vacuum. The spectral resolution was of 4 cm^{-1} and the FTIR spectra were recorded in the MIR wavenumber region going from 1000 to 4000 cm^{-1}. A three-electrode spectroelectrochemical cell, fitted with an MIR transparent flat window (CaF_2) at the bottom was used. The potentiostat was the same as used in CV experiments. The counter electrode was a glassy carbon slab, the working electrode consisted on the catalytic powder deposited over a glassy carbon disk (7 mm diameter) and a Reversible Hydrogen Electrode (RHE) was used as reference electrode. For the measurements 5 μL of the catalytic ink were deposited onto the glassy carbon substrate previously polished with alumina. To minimize the absorption of the infrared beam by the solution, the working electrode was pressed against the CaF_2 window during the acquisition and a thin layer of electrolytic solution was obtained. Two methods were used. The first one was the SPAIRS (Single Potential Alteration IR Spectroscopy), carried out in the potential range of 0.3–1.40 V *vs.* RHE at 1 mV s^{-1} and spectra were recorded every 0.05 V. The second one was a chronoamperometry/FTIRS study, performed at 0.8 V *vs.* RHE during 1 h with acquisition of spectra every 3 min. For each spectrum, 532 interferograms were co-added. The reflectance spectra were calculated for the different potential values as changes in the reflectivity (R_i) relative to a reference single-beam spectrum (R_0), as follows: $\Delta R/R = (R_i - R_0)/R_0$. The positive and negative bands represent a decrease and an increase in the number of species, respectively.

3.4 Chromatography and mass spectrometry measurements

Analytical investigations on glycerol conversion at the Pd-based electrode surface during long-term electrolysis were performed with high performance liquid chromatography (HPLC) with a semi-preparative ion exclusion column (Aminex HPX-87H). This liquid chromatography is also equipped with an UV-vis detector followed by a refractive index detector. At the end of long-term electrolysis in a two-compartment cell separated by anion exchange membrane, the recovered reaction products were neutralized on anion resin to remove the supporting electrolyte, and finally identified by LC-MS (Mass Spectrometry, Xevo Q-ToF, Waters) in negative ionization mode with an eluent that was water slightly acidified with formic acid (0.2%).

4. Conclusions

The identification of glycerol electrooxidation reaction products was performed using *ex situ* (LC-MS) and *in situ* (FTIR spectroscopy) complementary techniques. This provided evidence that this sustainable molecule can be used in a cogeneration process as fuel for renewable energy sources and as environmentally friendly raw material to produce added-value compounds. The results obtained show that palladium, 200 times more abundant that platinum on earth, when the distribution size is well controlled by microwave-assisted DPP synthesis method, can catalyse as well as other PGM electrode nanomaterials the glycerol oxidation in alkaline medium. Furthermore, the Mn and Fe content in the Pd catalyst composition effectively enhance the electrocatalytic glycerol reaction kinetics through tuning electronic structures and modifying highly active crystalline facets of palladium. This is supported by the high current densities and the shift of the onset potential toward lower values on PdM (M = Mn and Fe) electrodes. The oxidative glycerol conversion leads selectively to glycerate. Moreover and according to FTIRS measurements, the

preferential facets of the prepared Pd-based nanocrystals are capable of earlier removing the poisoning species such as CO from the electrode surface, which is facilitated by the oxygenated species of the Mn and Fe co-catalysts.

Acknowledgements

This work was mainly conducted within the framework of a collaborative program CAPES/COFECUB under Grant no. Ch 747-12. L. M. Palma acknowledges FAPESP foundation under contract number 2011/10213-6 for PhD scholarship.

Notes and references

1 Z. Zhang, L. Xin, J. Qi, D. J. Chadderdon and W. Li, *Appl. Catal., B*, 2013, **136–137**, 29–39.
2 L. Xin, Z. Zhang, J. Qi, D. Chadderdon and W. Li, *Appl. Catal., B*, 2012, **125**, 85–94.
3 Z. Zhang, K. L. More, K. Sun, Z. Wu and W. Li, *Chem. Mater.*, 2011, **23**, 1570–1577.
4 C. A. G. Quispe, C. J. R. Coronado and J. A. Carvalho Jr, *Renewable Sustainable Energy Rev.*, 2013, **27**, 475–493.
5 G. P. da Silva, M. Mack and J. Contiero, *Biotechnol. Adv.*, 2009, **27**, 30–39.
6 A. O. Costa, L. B. Oliveira, M. P. E. Lins, A. C. M. Silva, M. S. M. Araujo, A. O. Pereira Jr and L. P. Rosa, *Renewable Sustainable Energy Rev.*, 2013, **27**, 407–412.
7 C.-H. Zhou, J. N. Beltramini, Y.-X. Fan and G. Q. Lu, *Chem. Soc. Rev.*, 2008, **37**, 527–549.
8 X. Zhang and P. K. Shen, *Int. J. Hydrogen Energy*, 2013, **38**, 2257–2262.
9 S. E. Davis, M. S. Ide and R. J. Davis, *Green Chem.*, 2013, **15**, 17–45.
10 R. Dobson, V. Gray and K. Rumbold, *J. Ind. Microbiol. Biotechnol.*, 2012, **39**, 217–226.
11 Y. Kwon, Y. Birdja, I. Spanos, P. Rodriguez and M. T. M. Koper, *ACS Catal.*, 2012, **2**, 759–764.
12 S. Hirasawa, H. Watanabe, T. Kizuka, Y. Nakagawa and K. Tomishige, *J. Catal.*, 2013, **300**, 205–216.
13 W. Hu, D. Knight, B. Lowry and A. Varma, *Ind. Eng. Chem. Res.*, 2010, **49**, 10876–10882.
14 J. Xu, H. Zhang, Y. Zhao, B. Yu, S. Chen, Y. Li, L. Hao and Z. Liu, *Green Chem.*, 2013, **15**, 1520–1525.
15 N. Dimitratos, J. A. Lopez-Sanchez, J. M. Anthonykutty, G. Brett, A. F. Carley, R. C. Tiruvalam, A. A. Herzing, C. J. Kiely, D. W. Knight and G. J. Hutchings, *Phys. Chem. Chem. Phys.*, 2009, **11**, 4952–4961.
16 N. Dimitratos, J. A. Lopez-Sanchez and G. J. Hutchings, *Chem. Sci.*, 2012, **3**, 20–44.
17 D. Liang, J. Gao, J. Wang, P. Chen, Y. Wei and Z. Hou, *Catal. Commun.*, 2011, **12**, 1059–1062.
18 B. Katryniok, H. Kimura, E. Skrzynska, J.-S. Girardon, P. Fongarland, M. Capron, R. Ducoulombier, N. Mimura, S. Paul and F. Dumeignil, *Green Chem.*, 2011, **13**, 1960–1979.
19 Y. Kwon, K. J. P. Schouten and M. T. M. Koper, *ChemCatChem.*, 2011, **3**, 1–11.
20 G. L. Brett, Q. He, C. Hammond, P. J. Miedziak, N. Dimitratos, M. Sankar, A. A. Herzing, M. Conte, J. A. Lopez-Sanchez, C. J. Kiely, D. W. Knight, S. H. Taylor and G. J. Hutchings, *Angew. Chem., Int. Ed.*, 2011, **50**, 10136–10139.
21 Y. Zhang, X. Cui, F. Shi and Y. Deng, *Chem. Rev.*, 2011, **112**, 2467–2505.
22 S. Gil, N. Cuenca, A. Romero, J. L. Valverde and L. Sánchez-Silva, *Appl. Catal., A*, 2014, **472**, 11–20.
23 Z. Zhang, L. Xin, J. Qi, D. J. Chadderdon, K. Sun, K. M. Warsko and W. Li, *Appl. Catal., B*, 2014, **147**, 871–878.
24 E. Skrzyńska, J. Ftouni, A.-S. Mamede, A. Addad, M. Trentesaux, J.-S. Girardon, M. Capron and F. Dumeignil, *J. Mol. Catal. A: Chem.*, 2014, **382**, 71–78.
25 G. J. Hutchings and C. J. Kiely, *Acc. Chem. Res.*, 2013, **46**, 1759–1772.
26 F. Ksar, L. Ramos, B. Keita, L. Nadjo, P. Beaunier and H. Remita, *Chem. Mater.*, 2009, **21**, 3677–3683.
27 J. A. Lopez-Sanchez, N. Dimitratos, P. Miedziak, E. Ntainjua, J. K. Edwards, D. Morgan, A. F. Carley, R. Tiruvalam, C. J. Kiely and G. J. Hutchings, *Phys. Chem. Chem. Phys.*, 2008, **10**, 1921–1930.
28 S. Carrettin, P. McMorn, P. Johnston, K. Griffin, C. J. Kiely and G. J. Hutchings, *Phys. Chem. Chem. Phys.*, 2003, **5**, 1329–1336.
29 H. Zhang, M. Jin, Y. Xiong, B. Lim and Y. Xia, *Acc. Chem. Res.*, 2013, **46**, 1783–1794.
30 Z. Zhang, K. L. More, K. Sun, Z. Wu and W. Li, *Chem. Mater.*, 2011, **23**, 1570–1577.
31 P. K. Shen and C. Xu, *Electrochem. Commun.*, 2006, **8**, 184–188.
32 T. S. Ahmadi, Z. L. Wang, T. C. Green, A. Henglein and M. A. El-Sayed, *Science*, 1996, **272**, 1924–1925.
33 C. Koenigsmann and S. S. Wong, *ACS Catal.*, 2013, **3**, 2031–2040.
34 W. Yu, M. D. Porosoff and J. G. Chen, *Chem. Rev.*, 2012, **112**, 5780–5817.
35 M. A. Matin, J.-H. Jang and Y.-U. Kwon, *J. Power Sources*, 2014, **262**, 356–363.
36 Y. Holade, C. Morais, S. Arrii-Clacens, K. Servat, T. W. Napporn and K. B. Kokoh, *Electrocatalysis*, 2013, **4**, 167–187.
37 R. S. Ferreira Jr, M. Janete Giz and G. A. Camara, *J. Electroanal. Chem.*, 2013, **697**, 15–20.
38 Z. Zhang, L. Xin, K. Sun and W. Li, *Int. J. Hydrogen Energy*, 2011, **36**, 12686–12697.
39 S. Y. Shen, T. S. Zhao, J. B. Xu and Y. S. Li, *J. Power Sources*, 2010, **195**, 1001–1006.
40 C. Bianchini and P. K. Shen, *Chem. Rev.*, 2009, **109**, 4183–4206.
41 M. Grdeń and A. Czerwiński, *J. Solid State Electrochem.*, 2008, **12**, 375–385.
42 J. Fei, K. G. Lim and G. T. R. Palmore, *Chem. Mater.*, 2008, **20**, 3832–3839.
43 M. Huang and Y. Austin Chang, *J. Appl. Phys.*, 2006, **99**, 023527.

44 S. Yin, M. Takahashi, R. Miida, H. Iwasaki and K.-i. Ohshima, *Mater. Trans.*, 2011, **52**, 374–379.
45 Y. Liang, H. Zhang, Z. Tian, X. Zhu, X. Wang and B. Yi, *J. Phys. Chem. B*, 2006, **110**, 7828–7834.
46 S. Yin, L. Luo, C. Xu, Y. Zhao, Y. Qiang and S. Mu, *J. Power Sources*, 2012, **198**, 1–6.
47 M. Zhao, K. Abe, S.-i. Yamaura, Y. Yamamoto and N. Asao, *Chem. Mater.*, 2014, **22**, 1056–1061.
48 S. Song, Y. Wang, P. Tsiakaras and P. K. Shen, *Appl. Catal., B*, 2008, **78**, 381–387.
49 J. Qi, L. Xin, D. J. Chadderdon, Y. Qiu, Y. Jiang, N. Benipal, C. Liang and W. Li, *Appl. Catal., B*, 2014, **154–155**, 360–368.
50 D. Z. Jeffery and G. A. Camara, *Electrochem. Commun.*, 2010, **12**, 1129–1132.
51 Y. Holade, C. Morais, K. Servat, T. W. Napporn and K. B. Kokoh, *ACS Catal.*, 2013, **3**, 2403–2411.
52 T. S. Almeida, L. M. Palma, P. H. Leonello, C. Morais, K. B. Kokoh and A. R. De Andrade, *J. Power Sources*, 2012, **215**, 53–62.
53 B. D. Cullity and S. R. Stock, *Elements of X-Ray Diffraction*, New Jersey, 2001.
54 J. Ribeiro, D. M. dos Anjos, K. B. Kokoh, C. Coutanceau, J. M. Léger, P. Olivi, A. R. de Andrade and G. Tremiliosi-Filho, *Electrochim. Acta*, 2007, **52**, 6997–7006.